Multi-scale Approach Continuously Relating the Microstructure and the Macroscopic Mechanical Properties of Plaster Pastes during Their Settings

Hamouda Jaffel,[†,‡] Jean-Pierre Korb,*[,†] Jean-Philippe Ndobo-Epoy,[‡] Jean-Pierre Guicquero,[‡] and Vincent Morin[‡]

Laboratoire de Physique de la Matière Condensée, UMR 7643 du CNRS, École Polytechnique, 91128 Palaiseau Cedex, France and Lafarge, Centre de Recherche, 38291 Saint-Quentin Fallavier Cedex, France

Received: May 9, 2006; In Final Form: July 5, 2006

A new multi-scale experimental approach is proposed to continuously relate the microstructure and the macroscopic mechanical properties of plaster pastes during their settings. ^{1}H NMR relaxometry is used to follow continuously and not destructively, the degree of hydration and the microstructure evolution during the setting and hardening of plaster paste. Transmission of shear and compressional ultrasonic velocities enable the determination of macroscopic mechanical properties of the material during the setting. On the basis of similar behaviors of Young's modulus and NMR-population of confined water as function of the degree of hydration, we conclude that NMR gives a better understanding of the evolution of the microstructure at the origin of a better control of the macroscopic mechanical properties.

I. Introduction

How is it possible to relate quantitatively and nondestructively the microstructure of a porous medium to its macroscopic properties? Answering this question is of uttermost importance in civil engineering to control the mechanical properties of the materials. Here, we propose to investigate the case of gypsum, a material of general interest in the building industry. Our objectives are 2-fold: (i) Follow quantitatively, and without any perturbation, the hydration and setting of plaster, to get some key parameters such as the degree of hydration or the evolution of porosity as function of time; (ii) Relate these parameters to macroscopic mechanical properties (Young's, bulk and shear moduli...).

The determination of the relationships between micro- and macroscopic scales usually requires a large number of destructive experiments. Regarding the microstructure, mercury intrusion porosimetry (MIP) or nitrogen adsorption−desorption isotherms (BET) require a previous drying of the material, necessarily perturbing the evolution of the microstructure during the setting. Other techniques, such as X-rays tomography, SAXS, or SANS, enable the study of wet samples, but they require a synchrotron source and very thin nonrepresentative samples.[1] On the contrary, ^{1}H NMR relaxometry allows a nondestructive continuous probing of the water dynamics in the microstructure of porous materials.[2−4] It also enables the determination of the amount of water consumed during the setting and hardening of cement (or equivalent materials) and thus the degree of hydration.[5−9] Here, we propose a quantitative study of the microstructure of plaster pastes during their progressive settings by NMR relaxometry. Regarding the macroscopic mechanical properties, we use ultrasonic waves to probe, continuously and nondestructively, the evolution of the mechanical properties of plaster to avoid a large number of destructive compression tests. We succeed in relating these mechanical macroscopic measurements to the NMR microstructural ones. This study thus demonstrates the use of an experimental multi-scale approach that links microscopic measurements to macroscopic mechanical properties of a civil engineering material.

II. Materials and Methods

Calcium sulfate hemihydrate ($CaSO_4$, $1/2H_2O$), usually called plaster, comes from the dehydration of calcium sulfate dihydrate ($CaSO_4$, $2H_2O$), usually called gypsum. There are two varieties of plaster, α and β, produced by wet or dry methods, respectively. The plaster used in the experiments is a commercial β-plaster, 96 wt % pure hemihydrate (Meriel quarry, Lafarge Gypsum, France). The other impurities are mainly calcite, quartz, and gypsum.

The proton NMR relaxometry experiments are performed using a low field spectrometer (Maran-Ultra (0.55 T), Oxford Instruments Molecular Biotools, England), operating at the proton Larmor frequency of 23 MHz. The transverse relaxation decays are measured by the well-known Carr−Purcell−Meiboom−Gill (CPMG) sequence. For the kinetics studies (samples without addition of excess water), the echo time spacing is $2.\tau = 800$ μs (where τ is the 90−180° pulse gap) and the duration of the whole sequence is about 0.8 s. For the continuous determination of the NMR porosity (samples with addition of excess water), the echo time spacing is $2.\tau = 3000$ μs and the duration of the whole sequence is about 10 s. Each NMR sequence is accumulated four times and is repeated every minute during 2 h. Under theses conditions, we cannot detect the solid protons within the gypsum crystals and those chemically bound to the surface, since their relaxation times are far too short[4]. The samples were prepared by manual mixing of plaster powder with distilled water, at well-defined water-to-plaster weight ratios (w/p), from 0.4 to 1. The temperature regulation of the NMR apparatus is set to 25 °C.

* Corresponding author phone: 33 1 69 33 47 39; fax: 33 1 69 30 04; e-mail: jean-pierre.korb@polytechnique.fr.
† Laboratoire de Physique de la Matière Condensée.
‡ Centre de Recherche.

10.1021/jp062832a CCC: $33.50
Published on Web 08/30/2006

The calorimetric measurements are performed at 25 °C with an isotherm multichannel calorimeter (TAM Air, Thermometric, Sweden). We placed 3 g of plaster powder in a 10 mL flask in the calorimeter. The amount of water needed for each w/p is placed in syringes, just above the powder, inside the calorimeter. The powder and water are allowed to stabilize at 25 °C during 2 h before performing a manual mix of the powder and water inside the calorimeter, thanks to the use of a Teflon blade inside the calorimetric cell. This mixing system is sold with the Thermometric calorimeter. We follow the hydration heat flow for 2 h.

The macroscopic mechanical properties of the evolving microstructures are deduced from the continuous measurements of ultrasonic wave velocities. The ultrasonic setup is composed of a Plexiglas cell and a pair of 0.5 MHz transducers, generating and measuring both compressional and shear waves. These measurements allow the calculation of the elastic coefficients of the material[10−12] (bulk, shear, and Young's moduli). The transmitted ultrasonic waves generated by the Plexiglas/plaster paste interface are recorded every minute during 2 h, with a sampling frequency of 16 MHz. Complementary, the microstructures of polished sections of hardened gypsum, prepared with various water-to-plaster ratios w/p (1, 0.8, 0.6, and 0.4), are observed by SEM (JEOL 5800LV/Japan, operating at 15 kV), after impregnation with epoxy resin and metallization. The SEM pictures are binarized by Paint Shop Pro (Jasc Software), and the amount of black (voids) and white (solid) pixels are determined with Image Tool (UTHSCSA Software). This procedure gives us the evolution of 2D porosity as a function of w/p.

III. Results and Discussion

A. Measurement of the Degree of Hydration. At low magnetic fields and especially at long echo time spacing, the measured magnetization amplitude M_0 is proportional to the amount of free water molecules in the paste.[13,14] It is indeed well-known that solid protons within the hydrates (cement gel, gypsum dihydrate crystals) are chemically bound and cannot be detected since their relaxation times are far too short.[15,16] Consequently, the consumption of water during the hydration (formation of gypsum crystals) becomes directly related to the chemical degree of hydration, according to the following:

$$CaSO_4,\ 1/2H_2O_{(solid)} + 3/2\ H_2O_{(aq)} \rightarrow CaSO_4,\ 2H_2O_{(solid)} \quad (1)$$

For each NMR relaxometry experiment, t is the NMR acquisition time (from 0 to 0.8 s) and t_{hydr} the hydration time (from 0 to 120 min). The magnetization decay $M(t,t_{hydr})$ can be described by a multiexponential expansion:

$$M(t,t_{hydr}) = M(0,t_{hydr})\sum_i a_i(t_{hydr})\exp\left(-\frac{t}{T_{2i}(t_{hydr})}\right) \quad (2)$$

where $a_i(t_{hydr})$ are the corresponding magnetization fractions associated to the transverse relaxation times $T_{2i}(t_{hydr})$ as a function of the hydration time. The index i corresponds to the different water populations in the medium, each one having its own contribution to the whole signal. Usually, i is limited to 2 or 3 in the case of plaster paste.[4] To compare the different samples, we define the normalized NMR water magnetization $M_{norm}(t,t_{hydr})$ as a function of the hydration time by the following:

$$M_{norm}(t,t_{hydr}) = \frac{M(t,t_{hydr})}{M(0,0)} \quad (3)$$

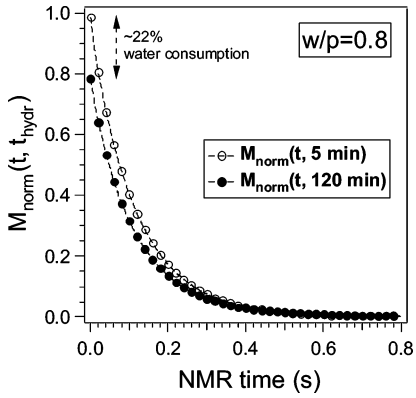

Figure 1. Normalized NMR transverse magnetization decays of a plaster paste ($w/p = 0.8$) at the beginning ($t_{hyd} = 5$ min) and at the end ($t_{hyd} = 120$ min) of the hydration.

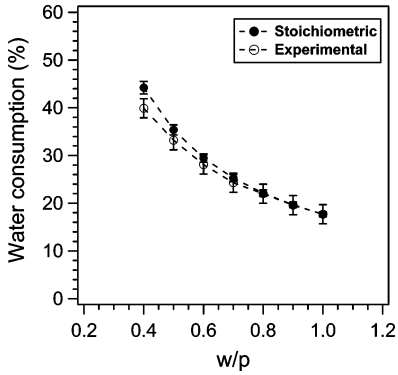

Figure 2. Water consumptions (as defined in the text) as a function of w/p.

where $M(0,0)$ is the extrapolated value of the total magnetization amplitude at the mixing time ($t_{hydr} = 0$), when plaster and water are initially mixed. Figure 1 shows the relaxation curves obtained by NMR relaxometry (CPMG sequence). The measurements are made after the mixing of plaster powder with distilled water, with a water-to-plaster weight ratio $w/p = 0.8$. The observed decrease of the magnetization amplitude (Figure 1) between the beginning ($t_{hydr} = 5$ min) and the end ($t_{hydr} = 120$ min) of the hydration enables the determination of the experimental water consumption at t_{hydr}: $1 - M(0,t_{hydr})/M(0,0)$. We aim at relating such a water consumption to a degree of hydration. Chemically, from eq 1, the water consumption is given by the stoichiometric ratio as $(w/p)_{stoi} = 0.186$. Usually, the paste is much too viscous at this ratio, and we are compelled to use an experimental water-to-plaster ratio $(w/p)_{exp}$ between 0.4 and 1. Thus, at a given $(w/p)_{exp}$ ratio, the "stoichiometric" water consumption is given by $(w/p)_{stoi}\varphi/(w/p)_{exp}$, where ϕ is the purity of the plaster. At the end of hydration ($t_{hydr} \rightarrow \infty$), we have

$$1 - \frac{M(0,t_{hydr} \rightarrow \infty)}{M(0,0)} = \frac{(w/p)_{stoi}}{(w/p)_{exp}} \times \varphi \quad (4)$$

In Figure 2, we compare the experimental and stoichiometric consumptions of water for different w/p ratios ($w/p = 1$, 0.9, 0.8, 0.7, 0.6, 0.5, and 0.4). We clearly see that the lower the w/p ratio, the higher the water consumption and the higher the difference between the stoichiometric and the experimental water consumptions. This difference can be explained by the very high viscosity of the paste at low w/p ratios, making it difficult to eliminate all the lumps, thus leading to a noncomplete hydration process after 2 h. To take the expected stoichiometric consump-

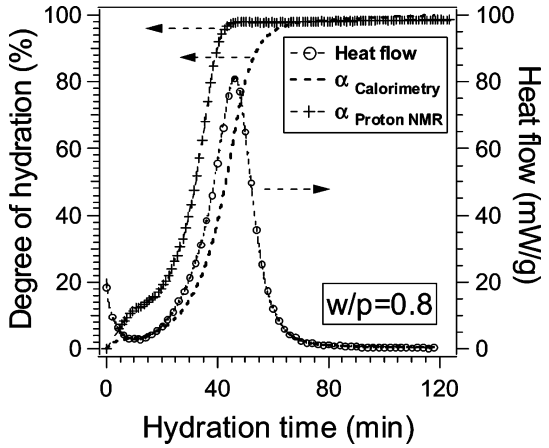

Figure 3. Comparison of the degrees of hydration obtained by NMR and isothermal calorimetry, both at 25 °C, and isothermal heat flow as a function of the hydration time for a plaster paste at $w/p = 0.8$.

tion of water into account, we define the NMR degree of hydration $0 \leq \alpha(t_{hydr}) \leq 1$ of the plaster paste by the following:

$$\alpha(t_{hydr}) = \left(1 - \frac{M(0,t_{hydr})}{M(0,0)}\right) \Big/ \left(1 - \frac{M(0,t_{hydr} \rightarrow \infty)}{M(0,0)}\right)$$

$$= \left(1 - \frac{M(0,t_{hydr})}{M(0,0)}\right) \Big/ \left(\frac{(w/p)_{stoi}}{(w/p)_{exp}} \times \varphi\right) \quad (5)$$

In Figure 3, we display the heat flow during the hydration of a plaster paste at $w/p = 0.8$ and the superposition of the degrees of hydration obtained by NMR ($\alpha_{protonNMR}$) and by isothermal calorimetry ($\alpha_{calorimetry}$). The heat flow curve in Figure 3 corresponds to the corrected data obtained by taking the time constant τ of the calorimeter (approximately 80 s) into account (first order correction: $signal_{corr} = signal_{raw} + \tau\ dsignal_{raw}/dt$). Since there is a competition between hemihydrate dissolution and gypsum crystallization during the whole hydration, three steps can be identified on Figure 3. The comparison of the calorimetric and NMR degrees of hydration shows an earlier linear increase of the NMR degree of hydration during the first 10 minutes. At this stage, the degree of hydration is limited by the dihydrate crystallization. After 10 min, we observe a sharp increase of both NMR and calorimetric degrees of hydration due to the exothermic development of a network of entangled gypsum needles. For $t_{hydr} \geq 45$ min, we observe a slight increase of the NMR degree of hydration corresponding to the end of the hydration. During this final step, the hydration is limited by the hemihydrate dissolution. Thus, the calcium sulfate concentration tends to the gypsum solubility (~2.65 g/L) by the crystallization of the last gypsum crystals.

We notice that the NMR degree of hydration is systematically shifted earlier than the calorimetric one, even after having taken the time constant of the calorimeter into account. A possible explanation of this difference is that a high amount of water molecules are adsorbed on the surface of hemihydrate during its wetting (corresponding to the wetting peak in the first minutes of the calorimetric heat flow). These water molecules are not detectable at long echo time spacing (highly bound solid protons behavior), leading to a "virtual" water consumption (i.e., water not consumed in the formation of gypsum crystals), and thus to an acceleration of the degree of hydration. The calorimetric degree of hydration seems slower because the higher weight comes from the formation of the network of gypsum needles beginning at 20 min, generating much more heat than the initial

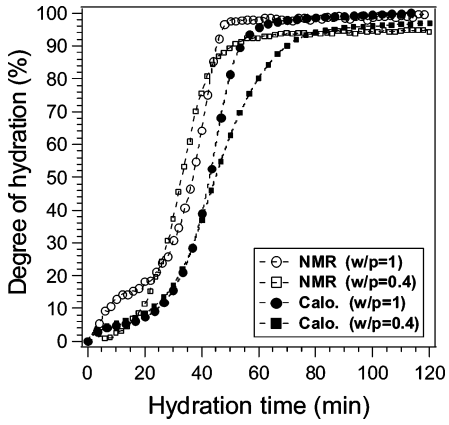

Figure 4. Comparison of the degrees of hydration obtained by NMR and isothermal calorimetry, both at 25 °C, as a function of hydration time, for plaster pastes at $w/p = 1$ and 0.4.

wetting of the powder. In a way, both NMR and calorimetric degrees of hydration are thus complementary. We checked that the systematic shift between both signals is not due to the difference of mixing the powder with water (external manual mix for the NMR, and internal manual mix for the calorimeter). For instance, we have performed a calorimetric measurement of a paste that has been externally mixed (like the NMR sample preparation) and do not observe any shift of the heat flow of the major peak. The main drawback of this external mix is that it prevents the study of the heat flow during the first 10 min due to the thermal equilibrium between the calorimeter and the sample. Nevertheless, at $w/p = 1$, the viscosity of the paste is low enough to lead to a homogeneous mix in both external and internal mixes. To go further, we display, in Figure 4, the comparison between NMR and calorimetric degrees of hydration for two extreme w/p ratios (0.4 and 1). First, by looking only at the NMR data in the first 20 min, we note that the hydration of plaster is lower at low w/p, due to a larger screening effect (tortuosity effect): the lower the w/p, the more difficult it is for the water molecules to diffuse in the medium. This is evidence that NMR is sensitive to the evolving microstructure during the hydration. On the contrary, we do not observe any significant difference between the calorimetric data in the first 20 min at these two extreme values of w/p. As mentioned above, the water consumption observed on the NMR data during the first minutes cannot be explained by the formation of gypsum crystals, since it should have given a sharp increase in the calorimetric data at about 10 min. The sigmoidal behavior of the calorimetric curves in the first 25 min can be explained by the competition of the exothermic dissolution of hemi-hydrate (dominant in the first 20 min), and the exothermic crystallization of gypsum (dominant after 20 min). After 30 min, the NMR data keep on being earlier than the calorimetric data, but with the same sigmoidal behavior, and achieve approximately the same hydration degrees at the end. For $w/p = 0.4$, only 95% of the hydration reaction is achieved after 2 h. This phenomenon has been previously interpreted by Sattler et al.[17] as the effect of a topotactical hydration taking place at low w/p ratios, i.e., gypsum microcrystallites with a high packing density, forming a trap for interstitial water.

From these results, we see that we can define a new degree of hydration from the NMR data that takes into account two preliminary stages before the reaction of crystallization: accessibility by diffusion to the reaction sites and creation of a surface population of highly bound protons. This new degree of hydration is especially useful at short hydration times.

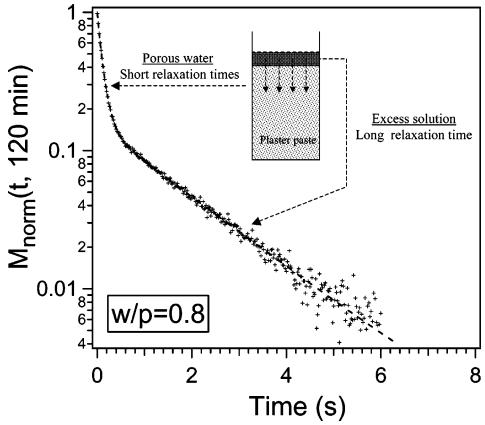

Figure 5. NMR transverse magnetization decay from the water filling the porosity and from the excess water added above a plaster paste ($w/p = 0.8$). Schematic diagram of the experiment (inset).

B. Probing the Development of the Microstructure. The hydration processes which take place during the hardening of plaster paste lead to two opposite phenomena: a contraction in volume (autogenous shrinkage), the volume of the hydration products being smaller than the sum of the volumes of plaster and mixing water, and a slight increase in the external volume (plaster swelling), due to the development of voids during the growth of gypsum crystals.[17] Since the low field NMR signal is proportional to free water in the material, the total NMR magnetization can be directly related to the evolution of the microstructure, and in particular to the porosity of the material, without any alteration of the system, provided that the pores are kept fully filled with water during the whole hydration. For that purpose, we have added a saturated solution of gypsum above the plaster paste. This addition was done a few minutes after the mixing in order to let the plaster begin to set and to avoid a variation of the *w*/*p* ratio. Figure 5 shows the transverse NMR magnetization of a sample composed of hardened plaster paste ($w/p = 0.8$) and an excess solution (2.65 g/L of $CaSO_4$). The porous volume can be easily deduced by a multiexponential decomposition of the total NMR magnetization decay. We use three exponentials: one for the excess water (long relaxation time, $T_2 \sim 2$ s), and two other ones for the water in large pores or confined in clusters of gypsum needles (short relaxation times, $T_2 \leq 200$ ms).[4] Consequently, measuring the proton NMR magnetization decays during the setting and the hardening of the plaster paste allows a continuous estimation of the total porosity $\Phi(\alpha)$ of the paste without any perturbation (no drying, no high pressure, and no perturbation of the hydration process). This porosity can be described as a function of the degree of hydration α by the following:

$$\Phi(\alpha) = \frac{V_{\text{pores}}(\alpha)}{V_{\text{pores}}(\alpha) + V_{\text{solid}}(\alpha)} \tag{6}$$

with,

$$\begin{cases} V_{\text{pores}}(\alpha) \propto \sum_i m_{i,\text{pores}}(\alpha) \\ V_{\text{solid}}(\alpha) = (1-\alpha)V_{\text{hemihydrate}}(0) + \alpha V_{\text{gypsum}}(1) \end{cases} \tag{7}$$

In eqs 6 and 7, $V_{\text{pores}}(\alpha)$ and $V_{\text{solid}}(\alpha)$ are the theoretical pores and solid phases volumes (hemihydrate ($V_{\text{hemihydrate}}$), dihydrate (V_{gypsum})) that both depend on the degree of hydration α. $V_{\text{hemihydrate}}(0)$ is the initially measured volume of hemihydrate, and $V_{\text{gypsum}}(1)$ is the theoretical gypsum volume for a complete hydration. $\sum_i m_{i,\text{pores}}(\alpha)$ is the sum of the magnetization amplitudes corresponding to the water confined in pores (not to the excess water) as a function of the degree of hydration. A comparison between eqs 2 and 7 gives $a_i = m_i/\sum_i m_i$.

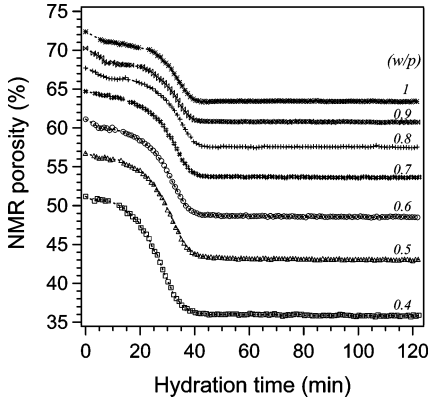

Figure 6. Time evolution of the measured "NMR porosity" of plaster pastes prepared with different water-to-plaster weight ratios ($w/p = 1$, 0.9, 0.8, 0.7, 0.6, 0.5, and 0.4).

TABLE 1: Porosities of Hardened Gypsum Samples Measured by Mercury Intrusion Porosimetry (MIP) and by ^{1}H NMR Relaxometry as a Function of the Water-to-Plaster Weight Ratio (*w*/*p*)

w/*p*.	0.4	0.5	0.6	0.7	0.8	0.9	1
Φ_{Hg} (%).	36	44	51	55	58	60	61
Φ_{NMR} (%).	36	43	49	54	58	61	63

Figure 6 shows the time evolution of the measured "NMR porosity" of the porous structures of plaster pastes prepared with several water-to-plaster ratios ($w/p = 1$, 0.9, 0.8, 0.7, 0.6, 0.5, and 0.4). Note that the term "porosity" can be debated while the setting of the material has not occurred (solid structure not well defined in a paste). Here, our low field "NMR porosity" refers quantitatively and without any perturbation to the volume available to free water molecules during the development of the microstructure. The only assumption is that the whole porosity is filled with water (no air bubbles). During the whole hydration process, we observe that the lower the *w*/*p* ratio, the lower the porosity of the pastes (higher amount of solid, denser material). For all the *w*/*p* ratios, the same sigmoidal behavior as a function of the hydration time is observed. The sharp decrease of the porosity at about 30 min is explained the same way as the degree of hydration (development of the gypsum crystals network).

We have compared the NMR porosities of the final solid microstructures of hardened gypsum with those obtained by mercury intrusion porosimetry (MIP) after drying the samples. In Table 1, we see that both NMR and MIP results after drying are quite similar. The net advantage of low field NMR is that it enables the continuous determination of the porosity of a sample at ambient pressure without any drying or the use of toxic mercury.

C. Macroscopic Mechanical Properties. We use the transmission of ultrasonic waves to collect continuously and nondestructively some information on the macroscopic mechanical properties of the microstructure of plaster paste during its setting and hardening. From the well-known theory of the acoustic wave propagation in elastic solids,[10] the Young's elastic modulus (E) of a material is as follows:

$$E = \rho V_T^2 \left(\frac{3V_L^2 - 4V_T^2}{V_L^2 - V_T^2} \right) \tag{8}$$

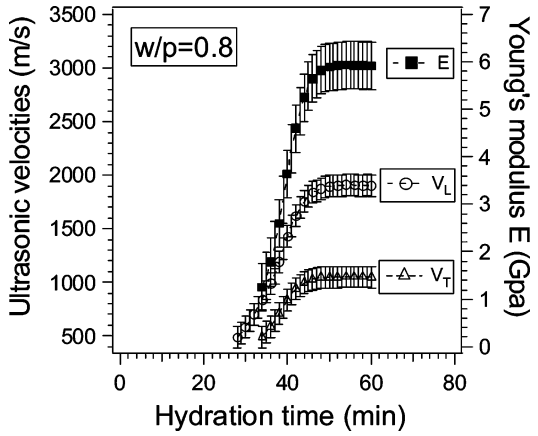

Figure 7. Time dependence of the ultrasonic velocities (V_T and V_L, corresponding to the shear and compressional waves, respectively) and the calculated (eq 8) elastic modulus E.

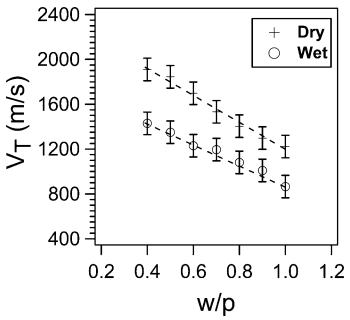

Figure 8. Evolution of the ultrasonic transverse velocity V_T as a function of w/p, for wet and dry samples.

where V_T and V_L are the measured velocities of shear (transverse) and compressional (longitudinal) ultrasonic waves and ρ is the plaster paste density. Figure 7 shows the time evolution of the Young's elastic modulus E of the evolving microstructure of a plaster paste ($w/p = 0.8$), deduced continuously from the ultrasonic shear (V_T) and compressional (V_L) wave velocities (using eq 8), also represented on Figure 7. The propagation of shear waves starts a few minutes after that of compressional waves, when a continuous path of grain is created through the paste. At $t_{hydr} \sim 35$ min, a sharp increase of the elastic Young's modulus is observed as a function of the hydration time following a sigmoidal behavior. This phenomenon is often associated with the microstructural percolation transition. In fact, during the setting and hardening, the microstructure changes from the state of a suspension of plaster particles of irregular shapes to the state of an interconnected solid phase that has well-defined elastic properties.

To see, macroscopically, the effect of the mixing parameter w/p ratio on these resulting elastic properties of the hardened materials, we measured the variations of ultrasonic shear (Figure 8) and compressional (Figure 9) wave velocities as a function of w/p. Wet and dry samples were studied to see if the mechanical behavior of the samples was altered by the wetting. This study was necessary to compare our NMR data (requiring wet samples) with the macroscopic mechanical properties in the dry state. Figures 8 and 9 show that the global behavior of the velocities as a function of w/p is not altered by the use of dry or wet samples. As expected, the lower the w/p or the dryer the samples, the higher the velocity. Consequently, the lower the porosity, the higher the elastic moduli of the samples.

The shear wave velocity (Figure 8) follows a quasi monotonic behavior as a function of the w/p ratio, indicating the existence of a percolated solid network whatever the w/p ratio. On the contrary, the compressional wave velocity (Figure 9) exhibits a bilinear behavior with a transition at $w/p \sim 0.7$.

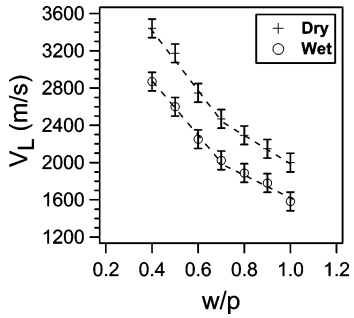

Figure 9. Evolution of the ultrasonic longitudinal velocity V_L as a function of w/p, for wet and dry samples.

D. Link Between Microscopic and Macroscopic Properties. This particular value of $w/p \sim 0.7$ has already been encountered in a previous study,[4] where NMR data showed the existence of two water populations in the porosity of hardened gypsum. We evidenced a step function for the exchange between these water populations, from no exchange for $0.4 \leq w/p \leq 0.6$ to a net exchange for $0.7 \leq w/p \leq 1$. But we had no macroscopic information on these materials. From the ultrasonic measurements described here (V_L as a function of w/p), a transition has also been observed at a macroscopic scale, at the same w/p ($\sim$0.7) as that observed by NMR. These similar behaviors at both microscopic and macroscopic scales are characteristic of a critical phenomenon, like a percolation occurring at a given threshold, here at $w/p \sim 0.6$ and 0.7. On the basis of our experiments, we assume the existence of a continuous percolation path of isolated gypsum crystals for $w/p > 0.6$, and a percolation path of gypsum crystals clusters for $w/p < 0.6$. Thus, the w/p ratio represents a key parameter, allowing a clear modification in both macro- and microstructure organizations.

To support this assumption, we have taken some SEM images of polished sections of hardened gypsum at different w/p ratios (1, 0.8, 0.6, and 0.4). Although these images (Figure 10) are 2D, we assume that a random cut of the material at a given w/p leads to the same 2D-image. These images exhibit a clear gap between $w/p = 0.8$ where gypsum crystals are poorly connected and $w/p = 0.6$ where those clusters are well connected. To go a step further, we have scanned and binarized 10 SEM images of polished sections of hardened gypsum for each w/p. Figure 11 shows the 2D porosity (% black) as a function of w/p. A change of the slope occurs at $w/p \sim 0.7$. We thus have another confirmation of the change of organization in the microstructure of plaster occurring at the same w/p as that observed by the NMR and ultrasonic experiments.

Figure 12 shows the evolution of the NMR porosity and the Young's elastic modulus (macroscopic parameters) as function of the chemical degree of hydration of the plaster, for a plaster paste at $w/p = 0.8$. As expected, the higher the degree of hydration, the lower the NMR porosity and the higher the Young's modulus. We note that the Young's elastic modulus E increases exponentially as a function of the degree of hydration. The best fit is obtained with a sigmoidal function.

Figure 13 shows the proton NMR water fractions P_1 and P_2 ($P_1 + P_2 = M(0, t_{hydr})/M(0, 0)$), as a function of the degree of hydration for a plaster paste at $w/p = 0.8$. The choice of a decomposition in two exponentials has been described in a previous paper.[4] On this figure, we clearly see a linear decrease of the water fraction P_1 as a function of the degree of hydration, parallel to a linear decrease of the total NMR porosity (Figure

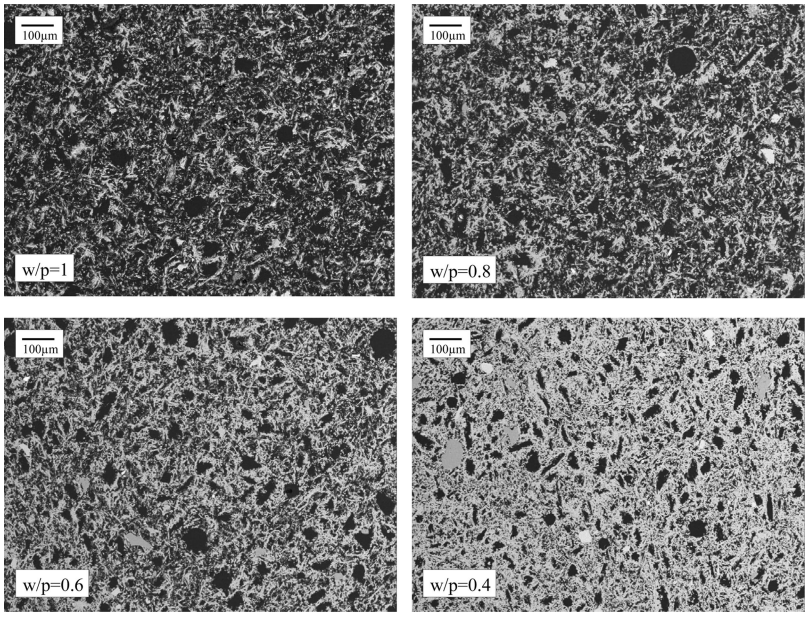

Figure 10. SEM photomicrographs of polished sections of hardened gypsum, prepared with different water-to-plaster weight ratios ($w/p = 1$, 0.8, 0.6, and 0.4). Bar length = 100μm. (white, solid; black, voids).

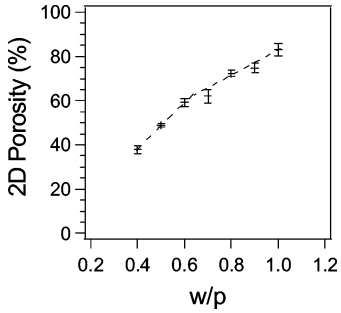

Figure 11. Evolution of the 2D porosity (% black) obtained by the binarization of the SEM images, as a function of the w/p ratio.

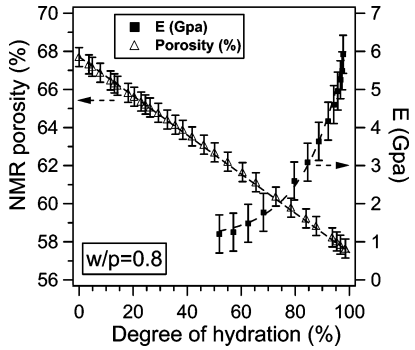

Figure 12. NMR porosity and ultrasonic Young's modulus plotted as a function of the NMR degree of hydration.

12), and to the beginning of the increase of the Young's modulus E. Over $\alpha = 90\%$, we observe an increase of the water fraction P_2, in parallel to the increase of the macroscopic Young's modulus of the material. Note that the sum of the water fractions equals 100% at $\alpha = 0$ (start of hydration) and ~78% at $\alpha = 1$ (end of hydration), as seen in Figure 1. Based on these multiscale results, we deduce that the less confined water population (P_1) is associated to bulk water saturating the interconnected porous volume. On the other hand, the more confined water population (P_2) is associated to the intercrystalline space, in clusters of growing needles shape crystals.

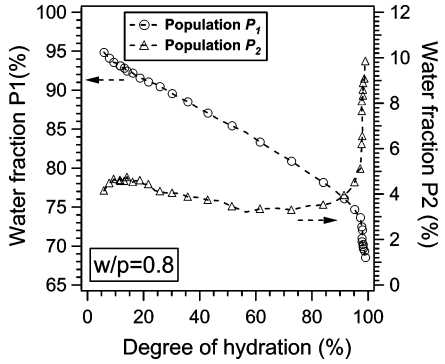

Figure 13. NMR water fractions P_1 (less confined) and P_2 (more confined) plotted as a function of the hydration time.

IV. Conclusion

We have presented a multiscale approach of the hydration and setting of the plaster paste. Using ^{1}H NMR relaxometry, a nondestructive characterization of the plaster hydration and a noninvasive determination of the resulting microstructure were successfully carried out. The main conclusions are the following: (i) A quantitative determination of the degree of hydration of plaster paste is determined continuously during the hydration from the water consumption, complementary to the traditional calorimetric measurements. (ii) A new method has been proposed to continuously probe the total porosity of the plaster paste during the setting. (iii) Ultrasonic waves were used to continuously probe the macroscopic mechanical properties of the plaster paste, such as the Young's modulus. (iv) A correlation between local measurements (obtained by NMR) and macroscopic properties (total porosity obtained by NMR and mechanical properties by ultrasound) has been established.

From this original multiscale approach, the increase of the Young's modulus as a function of the degree of hydration can be explained by the decrease of the less-confined water population and the increase of the more confined one. These populations can be quantitatively and continuously determined by NMR. We thus see that NMR helps us to better understand the evolution of the microstructure, and is a source of better

control of the macroscopic mechanical properties. We believe that the approach described here can be applied to the study of the setting of other reactive disordered materials.

References and Notes

(1) Allen, A. J.; Windsor, C. G.; Rainey, V.; Pearson, D.; Double, D. D.; Alford, N. M. *J. Phys. D: Appl. Phys.* **1982**, *15*, 1817.

(2) Halperin, W. P.; Bhattacharja, S.; D'Orazio, F. *Magn. Reson. Imaging* **1991**, *9*, 733.

(3) Korb, J. P. *Magn. Reson. Imaging* **2001**, *19*, 363.

(4) Jaffel, H.; Korb, J. P.; Ndobo-Epoy, J. P.; Morin, V.; Guicquero, J. P. *J. Phys. Chem. B* **2006**, *110*, 7385.

(5) Bhattacharja, S.; Moukwa, M.; D'Orazio, F.; Jehng, J. Y.; Halperin, W. P. *Adv. Cem. Based Mater.* **1993**, *1*, 67.

(6) Greener, J.; Peemoeller, H.; Choi, C.; Holly, R.; Reardon, E. J.; Hansson, C. M.; Pintar, M. M. *J. Am. Ceram. Soc.* **2000**, *83*, 623.

(7) Barberon, F.; Korb, J. P.; Petit, D.; Morin, V.; Bermejo, E. *Magn. Reson. Imaging* **2003**, *21*, 355.

(8) Nestle, N. *Solid State Nucl. Magn. Reson.* **2004**, *25*, 80.

(9) McDonald, P. J.; Korb, J. P.; Mitchell, J.; Monteilhet, L. *Phys. Rev. E* **2005**, *72*, 011409.

(10) Landau, L. D.; Lifshitz, E. M. *Theory of Elasticity*; Pergamon Press: Elmsford, NY, 1959.

(11) Boumiz, A.; Vernet, C.; Tenoudji, F. C. *Adv. Cem. Based Mater.***1996**, *3*, 94.

(12) Voigt, T.; Shah, S. P. *ACI Mater. J.* **2004**, *101*.

(13) Pel, L.; Kopinga, K.; Brocken, H. *Magn. Reson. Imaging.* **1996**, *14*, 931.

(14) Petkovic, J. *Moisture and Ion Transport in Layered Porous Building Materials: A Nuclear Magnetic Resonance Study*; Eindhoven University of Technology: Eindhoven, The Netherlands, 2005.

(15) Hansen, T. C. *Mater, Struct.* **1986**, *19*, 423.

(16) Valckenborg, R. M. E. *NMR on Technological Porous Materials*; Physique, Eindhoven University of Technology: Eindhoven, The Netherlands, 2001.

(17) Sattler, H.; Bruckner, H.-P. *ZKG Int.* **2001**, *54*.